Atmos. Meas. Tech. Discuss., 5, 5913–5951, 2012
www.atmos-meas-tech-discuss.net/5/5913/2012/
doi:10.5194/amtd-5-5913-2012

Atmospheric Measurement Techniques Discussions

Solar Backscatter UV (SBUV) total ozone and profile algorithm

P. K. Bhartia[1], R. D. McPeters[1], L. E. Flynn[2], S. Taylor[3], N. A. Kramrova[3], S. Frith[3], B. Fisher[3], and M. DeLand[3]

[1]Laboratory for Atmospheres, NASA Goddard Space Flight Center, Greenbelt, MD, USA
[2]NOAA NESDIS, College Park, Maryland, USA
[3]Science Systems and Applications Inc., Lanham, MD, USA

Received: 16 July 2012 – Accepted: 3 August 2012 – Published: 21 August 2012

Correspondence to: P. K. Bhartia (pawan.bhartia@nasa.gov)

Published by Copernicus Publications on behalf of the European Geosciences Union.

Abstract

We describe the algorithm that has been applied to develop a 41 yr time series of total ozone and ozone profiles from eight solar-backscatter UV (sbuv) instruments launched on NASA and NOAA satellites since April 1970. Although the basic algorithm is similar to the V8 algorithm that was released about a decade ago and has been in use since then at NOAA, the details of the V8 algorithm have never been published. The current version (V8.6) incorporates several changes including the use of new ozone absorption cross-sections and new ozone and cloud height climatologies. A particular emphasis in this paper is on characterizing the sources of errors that are relevant for deriving trends from monthly mean anomalies and for estimating biases between different types of ozone sensors. We show that variations in the local time of the measurement due to drifting NOAA satellite orbits can complicate the analysis of trends in the upper stratosphere. Such variations not only increase instrumental and algorithmic uncertainties but also require correction for true local time variations of ozone in the upper stratosphere and lower mesosphere for trend analysis. We find that the monthly zonal anomalies derived from the SBUV data have high precision, sufficient to track year-to-year changes in ozone over a broad range of altitudes. However, because of poor vertical resolution the data are less well suited to track short-term variability of ozone at lower altitudes.

1 Introduction

Systematic measurement of total column ozone and ozone profiles from space started with the launch of the BUV instrument on NASA's Nimbus-4 satellite in April 1970. Since then 9 additional instruments of progressively improved design have been launched on various NASA and NOAA satellites. The data produced by these instruments now span more than 41 yr with overlap among most instruments, except a 6-yr gap between the Nimbus-4 and Nimbus-7 satellites. Over the years several different

AMTD
5, 5913–5951, 2012

algorithms have been applied to process these data, but only a few have been published in the open literature (Bhartia et al., 1996). The current version of the algorithm (V8.6) is a modified version of the algorithm that was released in 2004 and has been in use at NOAA ever since.

In Sect. 2 we discuss the key features of the SBUV instrument relevant for developing the algorithm and understanding data quality. In Sect. 3 we provide details of the V8.6 algorithm. Section 4 discusses sources of error. In Sect. 5 we show comparisons between NOAA 17 SBUV/2 and Aura MLS instruments that have had several years of overlap.

2 SBUV instrument series

The SBUV instrument series consists of 10 instruments launched on 3 NASA and 7 NOAA satellites since 1970. Data from eight of these 10 instruments, shown in Fig. 1, are included in the current V8.6 dataset. Radiance data from the AE-E BUV instrument (launched in November 1975) are not available from the NASA archives for our use, although a study comparing AE-E BUV radiance data with models has been published (Prather, 1981). Data from the NOAA-19 SBUV/2 instrument (launched in February 2009) will be processed and added to the V8.6 dataset in 2012. In addition, the engineering model of the SBUV/2 instrument was flown as the shuttle BUV (SSBUV) instrument on eight NASA Space Shuttle missions during the period 1989–1996. These short duration missions were designed to validate the calibration of overflying SBUV/2 instruments (Hilsenrath et al., 1993). The SSBUV data have not been reprocessed using the V8.6 algorithm.

From an algorithm development perspective the design of these instruments has changed very little over the past 4 decades. All instruments view the earth in the nadir along the satellite track, with approximately $11.3^{\circ} \times 11.3^{\circ}$ field-of-view. They measure some 6 orders of magnitude change in the backscattered radiance between 250 and 340 nm by employing a double grating monochromator to minimize spectral straylight

AMTD
5, 5913–5951, 2012

from longer wavelengths and a photomultiplier tube (PMT) detector with multiple electronic gain ranges to provide high signal to noise ratio. In their primary operating mode, all instruments measure 12 discrete wavelength bands sequentially, with a triangular response function of 1.1 nm full-width at half maximum (Table 1). The measurement sequence takes 24 s to step through all 12 wavelengths (18 s for Nimbus-7 SBUV), which creates an effective footprint of 170 km × 340 km (200 km × 330 km for Nimbus-7). Beginning with Nimbus-7 SBUV, all instruments were modified to include a chopper wheel to reduce charged particle contamination and a continuous scan mode in which the instrument sweeps through the wavelength range 160–400 nm with 0.15–0.20 sampling (Heath et al., 1975). Continuous scan solar measurements have been used to monitor wavelength calibration.

The primary method of determining long-term instrument calibration of SBUV instruments is through measurement of the extra-terrestrial solar irradiance, obtained by using a reflective solar diffuser. Accurate tracking of changes in diffuser reflectivity has been a challenge, even though an on-orbit calibration system was added to the SBUV/2 instruments. DeLand et al. (2012) discuss these results in more detail. The long-term calibration of these instruments has therefore been supplemented by applying a variety of "soft" calibration techniques to characterize instrument response changes using carefully selected radiance data. For example, ice radiance measurements over Antarctica have been used to determine instrument degradation at 340 nm (Huang et al., 2003), and to correct any wavelength-independent bias in the radiance calibration. The overall spectral dependence of the response change is usually roughly linear between 250–340 nm, with larger degradation rates at shorter wavelengths (DeLand et al., 2012).

3 SBUV version 8.6 algorithm

Since the V8 algorithm was never formally published we describe the V8.6 algorithm using the V6 algorithm (Bhartia et al., 1996) as the basis for comparison. Bhartia

AMTD
5, 5913–5951, 2012

et al. (1996) provide many details regarding the information content of the UV radiances and discusses several heritage algorithms, including the "c-sigma" algorithm that solves the radiative transfer equation analytically to produce a 2-parameter ozone profile in the upper stratosphere (McPeters, 1980). The V6 algorithm was based on a two-step approach. The first step consisted of creating a good first guess profile using a simplified retrieval method. An upper stratospheric profile was created using the c-sigma method, and the lower profile was constructed by interpolating within a 21-profile dataset using total ozone derived from a pair algorithm (Klenk et al., 1982). These 21 profiles, popularly known as the TOMS standard profiles, vary with latitude and total ozone and capture a large fraction of the variance of the ozone profiles (Wellemeyer et al., 1997). Smoothly joined upper and lower profiles were used as a priori in step 2. The step 2 algorithm was based on a retrieval method proposed by (Twomey, 1963). Though Rodger's optimal estimation expression (Rodgers, 1976) was used in the actual software, the V6 algorithm was not strictly an optimum estimation (OE) technique. In OE the a priori error covariance should reflect the error associated with the a priori that is used. The V6 algorithm used a matrix whose terms were selected by trial and error, conceptually similar to the way one selects the γ-term in the Twomey algorithm to constrain the retrieval. By contrast, the V8 algorithm is a one step algorithm in which one uses a month/latitude climatology of ozone profiles constructed using various satellite and ozonesonde datasets as a priori (McPeters et al., 2007). Total ozone is derived by integrating the retrieved profile. Changes from V8 and V8.6 algorithms include new ozone (McPeters and Labow, 2012) and cloud height (Haffner, 2011) climatologies and change in ozone cross-sections. The following describes the details of the V8.6 algorithm.

3.1 Forward model

The forward model used to compute the top-of-the-atmosphere (TOA) radiances at SBUV wavelengths is essentially the same as that used in V6. It is based on the vector radiative transfer code developed by Dave (1964) with modifications to account for

AMTD
5, 5913–5951, 2012

molecular anisotropy by Ahmad and Bhartia (1995) and rotational Raman scattering (Ring effect) correction developed by Joiner et al. (1995). The primary difference is that we now use Malicet et al. (1995) ozone absorption cross-sections instead of those from Bass and Paur (1984). To account for the temperature dependence of the cross-section we use a month/latitude climatology of temperatures developed using NOAA temperature datasets. This climatology is also used to convert from a pressure to an altitude scale to account for the atmospheric curvature in computing the radiances. As in V6 the radiance is calculated assuming the atmosphere contains no aerosols. Aerosol scattering effects are indirectly estimated using a Lambertian reflectivity model (Dave, 1977, 1978). In this model the sun-normalized top-of-the-atmosphere radiance (I) in a cloud-free atmosphere is calculated using:

$$I = I_a + \frac{RT}{(1 - RS_b)} \quad (1)$$

where I_a is the purely atmospheric contribution and the 2nd term is the contribution from a Lambertian surface of reflectivity R. T is the diffuse plus direct solar radiance impinging on the surface times their transmittance to the satellite; and S_b is the surface to atmosphere backscatter fraction. Equation (1) is inverted to estimate R from sun-normalized 331 nm radiances (I_{331}) by

$$R = \frac{(I_{331} - I_a)}{[T + (I_{331} - I_a)S_b]} \quad (2)$$

Dave called the variable R so derived the Lambert-equivalent reflectivity (LER). Radiative transfer calculations show that in the absence of aerosols LER is close to the reflectance of the surface under ambient illumination in the relevant measurement geometry. The effect of aerosol is to increase R, and to introduce a spectral dependence depending upon its absorptive properties (Dave, 1978).

AMTD
5, 5913–5951, 2012

To account for clouds the TOA radiance is calculated by independent pixel approximation (IPA) in which one assumes that the scene consists of a mixture of two non-interacting scenes:

$$I = I_s(R_s, P_s)(1 - f_c) + I_c(R_c, P_c)f_c \quad (3)$$

where I_s is the TOA radiance calculated by assuming a Lambertian surface of reflectance R_s at pressure P_s, and I_c assuming an opaque Lambertian cloud of reflectance R_c at pressure P_c. Since both terms are calculated using the Lambertian approximation we call this model the Mixed LER (MLER) model. We estimate f_c from 331 nm radiances by inverting Eq. (3), assuming R_s of 0.15, $R_c$of 0.80, and climatological values of P_s and P_c. We use the LER model when f_c becomes negative or greater than 1, as well as for snow/ice. Both R & f_c are assumed to be wavelength independent for computing the radiances at other wavelengths. Since the 2nd term on the right side of Eq. (3) assumes an opaque cloud, it does not account for photons scattered by the atmosphere and surface below the cloud that pass through the cloud. The MLER model accounts for this contribution through the 1st term, since the f_c derived from Eq. (3) becomes smaller than the geometrical cloud fraction for clouds with reflectance smaller than 0.8. Mie scattering calculations (Ahmad et al., 2004) show that this approach works quite well in computing the λ-dependence of TOA radiance in presence of clouds.

As in V6, T and S_b are tabulated, while I_a is calculated as the sum of two terms: the single scattering term is calculated on-line using a spherical radiative transfer code (Bhartia et al., 1996) and the multiple scattering term is obtained by table look-up. Since the multiply-scattered and reflected component of radiances (MSR) vary largely with total column ozone and have a weak dependence on ozone profile, the MSR tables are created using the 21 TOMS standard profiles discussed earlier. Though in V6 we made no correction to these radiances for the difference between the standard profile and the retrieved profile, we now apply a first order Taylor series correction for this difference using Jacobians that are similarly tabulated. We compute the radiances at

AMTD
5, 5913–5951, 2012

0.1 nm intervals and then band average them to create the tables for the 1 nm instrument bandpass. Though this method was developed for the slow computers of earlier years, we have not seen any reason to change it since it produces accurate radiances and allows us to reprocess the entire SBUV record in a short time.

3.2 Inverse model

The inverse model is based on the optimum estimation formula of Rodgers (1976), designed for retrievals where the numbers of layers are larger than the number of wavelengths:

$$\hat{\mathbf{X}}_{n+1} = \mathbf{X}^{\mathrm{a}} + \mathbf{S}\mathbf{K}_n^T \left(\mathbf{K}_n \mathbf{S}\mathbf{K}_n^T + \mathbf{S}_\varepsilon\right)^{-1} \left[Y - \mathrm{Y}_n - \mathbf{K}_n \left(\mathrm{X}^{\mathrm{a}} - \hat{\mathrm{X}}_n\right)\right] \quad (4)$$

where $\hat{\boldsymbol{X}}_n$ is the state vector (ozone profile) retrieved in the nth iteration, $\boldsymbol{Y}$ is the measurement vector, $\mathbf{K}$ is the Jacobian $|\frac{\partial y}{\partial x}|$, X_{a} is the a priori profile, $\mathbf{S}$ is the covariance matrix, representing the assumed variation of the true profiles with respect to a priori, and $\mathbf{S}_\varepsilon$ is the covariance matrix of measurement errors. (We use the lower case to represent the elements of a matrix and the upper case for the matrix.) In V6 we used the logarithm of layer ozone as x to prevent layer ozone from becoming negative. However, this can produce a systematic bias in situations where the error in the retrieved value is larger than the value itself. Such situations typically occur in the ozone hole conditions. Therefore, starting with V8, we assume that x is the layer column ozone density.

The state vector $\boldsymbol{X}$ consists of ozone in 80 layers of equal log pressure, 20 layers per decade of pressure, covering 1 to 10^{-4} atm (1 atm = 1013.25 hPa), plus a top layer that extends to zero atm. We use these fine layers for quadrature accuracy. Since the vertical resolution of the retrieved profiles is much coarser, we report them in 21 layers by combining ozone in 4 layers to reduce from 80 to 20 layers plus the top layer. We shall call them SBUV layers. The pressure at the bottom of SBUV layer L is $10^{-(L-1)/5}$ atm; each layer being ~ 3.2 km thick. We also provide ozone mixing ratio

AMTD
5, 5913–5951, 2012

in standard pressure levels, calculated by differentiating the cumulative ozone profile (Fig. 2).

The measurement vector $\boldsymbol{Y}$ consists of N-values, where $N = 100\log_{10} I$ and I is the sun-normalized radiance. N-values are a measure of atmospheric attenuation, expressed in tenths of decibels; 1 N-value increase represents a 2.3 % decrease in I. Depending upon the instrument and solar zenith angle, the dimension of $\boldsymbol{Y}$ varies from 6 to 9. The longest SBUV band centered at 340 nm wavelength is currently not used. Since 331 nm is used to estimate R/f_c, as described in Sect. 3.1, it is not included in $\boldsymbol{Y}$. For Nimbus-4/BUV and Nimbus-7/SBUV the shortest wavelength, centered at 253.7 nm, was contaminated by NO gamma-band emission (McPeters, 1989). Though this wavelength was changed to 252 nm in subsequent instruments to avoid the contamination, the behavior of several NOAA SBUV/2 instruments at this wavelength has been erratic. To maintain long-term consistency we do not use this wavelength in the present algorithm. The longest wavelength used varies from 302 nm at small solar zenith angles (SZA) to 317.5 nm at large SZAs. This was done to minimize the effect of smoke and mineral dust aerosols that have very high absorption in the UV (Torres and Bhartia, 1999).

Since SBUV data are typically analyzed by computing the monthly zonal mean (MZM) of ozone, we considered retrieving MZM ozone directly using the MZM of N-values. Though the N-values vary almost linearly with layer ozone at most SBUV wavelengths, at some wavelengths (e.g., 302 nm) the non-linearity becomes too large for accurate retrieval using this method. So, while we continue to do individual profile retrievals, we have optimized the algorithm for MZM retrieval by constructing the **S** matrix to reflect the variability of MZMs rather than of individual profiles. Aura/MLS data show that the fractional standard variation of MZM anomalies (difference from climatology) is roughly independent of altitude, latitude and season, and the variations are highly correlated in adjacent layers. Hence in constructing the **S** matrix we assume that layer ozone has a constant fractional variation (σ) in all layers with a correlation length of 12 layers ($\sim$ 10 km), which gives $\mathbf{S}(i\,j) = \sigma^2 x_i^{\mathrm{a}} x_j^{\mathrm{a}} e^{-|i-j|/12}$, where i and j are layer

AMTD
5, 5913–5951, 2012

numbers. We also assume that the measurement uncertainties (σ_ε) are uncorrelated, independent of wavelength or signal level, which gives $\mathbf{S}_\varepsilon = \sigma_\varepsilon^2 I$. In this formulation the algorithm becomes very similar to the Twomey algorithm (Rodgers, 1990; Twomey, 1963) with $\gamma = (\sigma_\varepsilon/\sigma)^2$. We have selected γ of 0.754 (or 4×10^{-4} if the radiance error is converted from *N*-value to fractional error) by examining the sensitivity of the algorithm to expected errors in instrument calibration. Since we retrieve individual profiles rather than the MZM we assume rather large values for σ (=0.5) and σ_ε (=0.43*N*, or 1 % of radiance) in the processing software for detecting anomalous measurements. However, only the value of γ, and to a lesser extent the correlation length, affects the actual retrieval.

We note that it is possible to optimize the SBUV algorithm for the retrieval of short-term variability by constructing **S** and $\mathbf{S}_\varepsilon$ differently. Since short-term σ varies by more than an order of magnitude with altitude, latitude, and season the **S** matrix should reflect this variation. Similarly, the $\mathbf{S}_\varepsilon$ matrix should reflect the instrument and cloud-caused noise that varies with wavelength and signal level. Such algorithms have been developed for other UV instruments (Liu et al., 2005, 2010).

3.3 Information content

Rodgers (2000) discusses a variety of methods to characterize the information content of atmospheric profiles retrieved using inverse methods. However, his focus is largely on individual measurements rather than on the ensemble mean of retrieved profiles. In the following we have adapted his concepts for understanding the information contained in the MZM of ozone profiles retrieved from SBUV measurements and to provide guidance on how best to use these data for comparison with other instruments, trend analysis, and model validation.

AMTD
5, 5913–5951, 2012

3.3.1 Smoothing kernels

In absence of measurement errors the relationship between the truth profile (X) and the retrieved profile ($\hat{X}$) can be expressed as,

$$\hat{x}_i - x_i^{\mathrm{a}} = \sum_j w_{ij}\left(x_j - x_j^{\mathrm{a}}\right) \tag{5}$$

$$\mathbf{W} = \mathbf{S}\mathbf{K}_n^T\left(K_n\mathbf{S}\mathbf{K}_n^T + \mathbf{S}_\varepsilon\right)^{-1}\mathbf{K}_n \tag{6}$$

W acts as a low pass filter to convert the true anomaly (difference between the truth profile and SBUV-assumed climatology) into the retrieved anomaly. Since the elements of **W** can have large positive and negative values and its rows do not sum to 1, Eq. (5) produces a weighted sum rather than the average of the true anomalies, therefore, we shall call them Integrating Kernels (IKs). One can construct other filters depending on one's intended application. To get the more traditional bell-shaped filters, one can rewrite Eq. (5) as,

$$\frac{(\hat{x}_i - x_i^{\mathrm{a}})}{\hat{x}_i} = \sum_j a_{ij}\frac{(x_j - x_j^{\mathrm{a}})}{\hat{x}_j}, \text{ where, } a_{ij} = w_{ij}\frac{\hat{x}_j}{\hat{x}_i} \tag{7}$$

The matrix **A** with elements a_{ij} smoothes fractional anomalies. For consistency with previous usage of this term we shall call them Averaging Kernels (AKs), even though the rows of **A** do not sum to exactly 1. To smooth mixing ratio anomalies one can replace x_i with $m_i p_i$ in Eq. (5), where m_i is the average MR in layer i and p_i is the pressure at mid point of the layer. The elements of the smoothing matrix in this case become $w_{ij}p_j/p_i$. We refer to all such filters as Smoothing Kernels (SK). Since SKs of variety of different shapes can be created simply by coordinate transformation, the shapes of the SKs are obviously not important. However, the diagonal elements of SKs are invariant under such transformations, so they are more robust and easier to interpret. We will discuss them in the next section.

AMTD
5, 5913–5951, 2012

Figure 3 compares two forms of SKs that we have found most useful. The AKs are useful for smoothing individual profiles in the upper upper stratosphere, where the kernels are well defined and are centered at the correct pressure level. The IKs are more useful for smoothing layer ozone amounts, particularly in the lower layers where the layers need to be combined to produce useful results from SBUV. They are also useful for analyzing MZMs. Since **W** is nearly independent of $X - X^{a}$, one can smooth MZM anomalies using the following expression:

$$\left(\overline{\hat{X}} - X^{a}\right) = \overline{\mathbf{W}}\left(\overline{X} - X^{a}\right) \tag{8}$$

where, the horizontal bars represent MZM. For this reason we provide $\overline{\mathbf{W}}$ on the MZM files (SBUV orbital files contain the more familiar AKs. Note that for historical reasons some SBUV documents may refer **W** as AK and **A** as fractional AK. Our use of terms IK and AK for these kernels is designed to eliminate this confusion).

3.3.2 Degrees of Freedom of the Signal (DFS)

Rodgers refers to the sum of the diagonal elements of the averaging kernels as DFS. DFS values plotted in Fig. 4 provide an estimate of the independent pieces of information that the algorithm is capable of retrieving. Note that DFS cannot exceed the number of wavelengths used, which varies from 6 at low SZAs to 9 at large SZAs. Figure 5 shows the diagonal elements of **W** (layer DFS). Since $1/w_{ii}$ is roughly the vertical resolution of the retrieved profile in unit of layers (converted to ~km by multiplying with 3.2), we have chosen the layering scheme for reporting SBUV profiles such that the maximum DFS of a layer is ~0.5, which provides roughly two data points per resolution element to meet Nyquist sampling criterion. Figure 5 shows that the vertical resolution of SBUV profiles varies considerably from layer to layer. This complicates the analysis and interpretation of SBUV data. The recommended procedure for comparing SBUV data with models and other measurements is to compare anomalies smoothed

AMTD
5, 5913–5951, 2012

using Eqs. (5)–(8). However, as the DFS of a layer goes down (resolution gets worse) interpretation of SBUV data gets increasingly difficult. An alternative is to combine multiple layers to create thicker layers. However, the advantage of doing so may or may not be significant. Firstly, when layers i_1 thru i_2 are combined the DFS of the combined layer (assuming that the fractional standard deviation of ozone is independent of layer no.) is given by $\frac{\sum_{i=i_1}^{i_2} x_i \sum_{j=i_1}^{i_2} w_{ij}}{\sum_{i_1}^{i_2} x_i}$. Because of the weighting by x_i, this is typically not much larger than the DFS of the layer for which x_i is the largest. Secondly, thicker layers usually have smaller fractional variability. So the signal to noise may not improve, and may even get worse, when layers are combined.

3.3.3 Column integrating kernels

From Eq. (5) it is easy to construct smoothing kernels ($\boldsymbol{W}^{\mathrm{c}}$) for the anomalies of any partial column. For the partial ozone column obtained by summing layers i_1 through i_2 the elements of $\boldsymbol{W}^{\mathrm{c}}$ are given by $\boldsymbol{W}^{\mathrm{c}}_i = \sum_{j=i_1}^{j=i_2} w_{ij}$. For perfect retrieval $\boldsymbol{W}^{\mathrm{c}}$ should be 1 in layers i_1 though i_2 and zero elsewhere. Though, strictly speaking, this does not occur for any layer combination, the IK for total column ozone comes very close to the ideal (Fig. 6). Note that this occurs despite the fact that the DFS of the lower SBUV layers is quite small. The reason is that while the algorithm does not have the vertical resolution to distinguish between tropospheric and stratospheric changes, the measured radiances are quite sensitive to tropospheric ozone variability. To explain the measurements the algorithm distributes the tropospheric changes over a wide range of altitudes to minimize the fractional deviation of the retrieved profile from the a priori profile.

AMTD
5, 5913–5951, 2012

4 Error analysis

Algorithmic errors in retrieved profiles from remote sensing instruments such as SBUV tend to be spatially and temporally correlated. Therefore, as data are averaged truly random errors such as instrument noise quickly become insignificant compared to non-random errors. On the other end of the error spectrum are systematic errors that do not vary significantly from year-to-year. Typical examples are errors in ozone absorption cross-section or in various climatologies used in the retrieval. Though biases produced by such errors often get lot of attention they are usually of little importance for the study of inter-annual variability and trends from a single instrument type. However, they do become important for combining data from different instruments. Since such complexity cannot be handled simply by providing accuracy and precision numbers we discuss below errors that are specific for particular application.

4.1 Errors in deriving Inter-annual variability and trend

From Eq. (5), in absence of instrument error, the error in MZM anomaly (deviation from long-term mean of SBUV data themselves, not from a priori) is given by,

$$\Delta\hat{X} = (1 - \overline{\mathbf{W}})\Delta X \tag{9}$$

The covariance matrix of this error, called smoothing error, is given by $(I - \overline{\mathbf{W}})\mathbf{S}_z(I - \overline{\mathbf{W}})^T$, where $\mathbf{S}_z$ is the covariance matrix of the true MZM anomalies of ozone in SBUV layers. We provide the square root of the diagonal elements of these errors in the SBUV MZM files. To do this calculation we use $\mathbf{S}_z$ estimated from Aura/MLS and ozonesonde data. Figures 7 and 8 show estimated errors in retrieved profiles and total ozone respectively for some typical cases.

In addition to smoothing errors one also may have errors in measuring and computing the radiances. The contribution of these errors to MZM anomaly is given by $\overline{\mathbf{G}}\varepsilon_N$, where ε_N is the MZM anomaly of N-value errors, and $\mathbf{G}$ is given by:

AMTD
5, 5913–5951, 2012

$$\mathbf{G} = \mathbf{S}\mathbf{K}_n^T \left(\mathbf{K}_n \mathbf{S}\mathbf{K}_n^T + S_\varepsilon\right)^{-1} \quad (10)$$

To apply Eq. (10) to estimate profile errors one needs to know ε_N. Of course, if one knew ε_N one would have corrected it. So the primary value of **G** is to assess if a model of instrument behavior derived from other means, including comparison with other datasets, is consistent with the measurement. A useful way to do so is to look at the time dependence of the final residuals (r_f), which is defined as the difference between measured N-values and those calculated from the retrieved profile. The following expression provides the relationship between the two.

$$r_f = (1 - K_n^* \mathbf{G})\varepsilon_N \quad (11)$$

where **G** is calculated from Eq. (10) using **K** whose column is set to zero if the corresponding wavelength is not used in the retrieval, while $\mathbf{K}^*$ is calculated at all wavelengths to provide the residuals at all wavelengths. For an assumed ε_N one can calculate the residuals using Eq. (11) and compare with retrieved values to see if they agree. Figure 9 shows the effect of a linearly varying error in N-values on retrieved O_3 and residuals estimated using Eqs. (10) and (11). Analysis of such residuals has been very useful in detecting and assessing SBUV instrument errors (DeLand et al., 2012).

Finally, we need to consider an effect that is unique to SBUV/2 instruments on NOAA satellites. Though these satellites were launched in a nominal sun-synchronous orbit, they measured at a fixed local time at any given latitude only over short time periods (1–2 yr); the local times of measurements drifted over longer time periods (McPeters et al., 2012). This drift creates a MZM anomaly in solar zenith angles. Since the property of the SBUV algorithm varies considerably with solar zenith angle, including the number of wavelengths used and the DFS, the orbit drift can alias time independent errors into time dependent errors. Though we expect that these errors are small, further work needs to be done to quantify them.

AMTD
5, 5913–5951, 2012

4.2 Systematic errors/biases

There are several sources of systematic errors that can create time independent (but month and latitude dependent) bias in the SBUV retrieved profiles. They include errors in a priori profiles, in measured and calculated N-values, and in various climatologies used in the forward model.

An error ΔX^a in a priori profile introduces a bias in the retrieved profile given by, $\Delta\hat{X} = (I - \mathbf{W})\Delta X_a$. Since ($I$-**W**) acts as a high pass filter, low vertical resolution errors in X^a, such as biases that vary slowly with altitude, are filtered out by the algorithm. By contrast high vertical resolution errors, such as incorrect tropopause height or mixing ratio peak will affect the retrieval. Though such errors are reduced by providing SBUV profiles in ~ 3.2 km thick layers, they are not eliminated completely. For example a layer with DFS of 0.3 will transmit 70 % of the bias in X^a in that layer to the retrieved profile. But if the fractional bias is the same in adjacent layers its impact on the retrieved profile is reduced.

Errors in measured N-values include calibration errors that typically do not vary with latitude, but may include other errors that do, e.g., non-linearity and straylight. Since SBUV uses double monochromator with a single detector the spectral and spatial straylight errors are small. For more details on the characterization of SBUV instruments see DeLand et al. (2012).

Since the UV ozone absorption cross-section varies with temperature, an error in the assumed temperature climatology will introduce an error in calculating the N-values. This error is minimized for SBUV since SBUV does not use measurements in the Huggins ozone absorption band where the temperature sensitivities are large (Table 1). Other sources of error in computing the N-values include polar mesospheric clouds (DeLand et al., 2003), stratospheric aerosols produced by volcanic eruptions (Torres and Bhartia, 1995), volcanic SO_2 (McPeters, 1993), and UV-absorbing aerosols, that include ash, smoke, and desert dust (Torres and Bhartia, 1999). The latter effects are small at wavelengths used in the SBUV retrieval. The effect of stratospheric aerosols

AMTD
5, 5913–5951, 2012

are very strongly dependent on the aerosol altitude; aerosols below ~ 20 km have relatively small effect but aerosols at higher altitudes can cause significant underestimation of layer ozone (Torres and Bhartia, 1995). During the 41-yr record of SBUV measurements there were only two volcanic eruptions that injected significant amounts of aerosols above 20 km: the April 1982 eruption of El Chichon, and the June 1991 eruption of Mt. Pinatubo. Some of the worst affected profiles and MZMs are caught by internal checks that we have built into the algorithm. The errors that remain need further study.

4.3 Diurnal variation of ozone

As discussed earlier, the local time of measurements from NOAA SBUV/2 instruments drifted over the lifetime of the instruments. Though the retrieval errors caused by these drifts are probably small, it should be noted that the data from these instruments are affected by the true diurnal (daytime) variation of ozone. For extraction of long-term trends from these instruments such variations need to be considered in the analysis of SBUV data. Though day to night variation of mesospheric ozone is well known, variations of ozone during daylight hours are not well established (Haefele et al., 2008; Huang et al., 2010). Several ground-based microwave radiometers (MWR) radiometers, which are part of the Network for the Detection of Atmospheric Composition Change (NDACC), acquire ozone profile data throughout the day at roughly the vertical resolution of SBUV. Recent reanalysis (Alan Parrish, private communication) of the NDACC/MWR data from the Mauna Loa Observatory (MLO) suggests that ozone mixing ratios vary by 3–10 % between 0.5 and 10 hPa over the local times when SBUV/2 data have been acquired. The phase of the variation changes from a mid-afternoon minimum at and above 1.5 hPa to an afternoon maximum below. In addition, Aura/MLS has provided ozone profiles at 01:30 a.m. and 01:30 p.m. local times over the entire globe since late 2004. We plan to combine these results with numerical models to construct a model of diurnal variation of ozone that can be used to normalize the SBUV measurements to a noon local time for the purpose of trend analysis.

AMTD
5, 5913–5951, 2012

5 Results

Since this paper focuses on the SBUV algorithm rather than on validation and data interpretation, we will limit our discussion of the SBUV results to just the NOAA 17 SBUV/2 instrument that had good overlap with Aura/MLS. Both instruments have performed quite well in space with Aura/MLS providing one of the most comprehensive moderate vertical resolution (~ 3 km) datasets of ozone profiles available to compare with SBUV (Froidevaux et al., 2008). More importantly, MLS profiles are provided in pressure vs. MR coordinate, which can be converted to SBUV layer ozone without using temperature profiles. The best ozone profile datasets available prior to MLS came from occultation instruments, such as SAGE, that retrieve ozone density as a function of altitude. Though they have been converted into pressure vs. MR scale, the conversion depends upon a NOAA stratospheric temperature record that is not of very high quality, particularly in the upper stratosphere. Finally, since MLS provides data in daytime around 01:30 p.m. local time, while NOAA 17 SBUV/2 measured around 09:30 a.m. local time, the diurnal variation is less of a problem in comparing SBUV with MLS than it is for occultation instruments.

Figure 10 shows that the bias between SBUV and smoothed MLS anomalies (calculated using Eq. 5) is less than 5 %. Since this procedure removes any bias introduced by errors in SBUV a priori, these biases are due to combined error in SBUV and MLS measurements and forward model, e.g., O_3 absorption cross-section. Converting these biases into an estimated SBUV N-value error reveals latitude and wavelength dependent errors that we think are unlikely to be in SBUV measurements. Though biases in mesospheric O_3 could be due to the 4 h difference in the local time of the two measurements, assigning the bias in the lower stratosphere to SBUV or MLS requires comparison with ozonesondes.

Figures 11 thru 13 show statistical analyses of SBUV and MLS-derived inter-annual variability of layer ozone and partial O_3 column above various pressure levels with and without smoothing MLS anomalies. Although most results are as expected based on

AMTD
5, 5913–5951, 2012

the DFS analysis presented in Sect. 3.3, poor performance of SBUV at ~ 20 hPa in the tropics when compared with unsmoothed MLS data is a surprise. Although a detailed analysis of this error is outside the scope of this paper, the error is caused by the fact that most of the inter-annual variability in O_3 at ~ 20 hPa is due to QBO (Kramarova et al., 2012). Since the QBO phase varies with altitude, vertical smoothing causes a distortion of the phase in SBUV data, which then appears as noise when compared with unsmoothed MLS data.

6 Summary and conclusions

We have described the algorithm that has been used to reprocess data from 8 instruments in the SBUV instrument series launched since April 1970. The algorithm has been optimized for retrieving monthly zonal mean (MZM) profiles by constructing appropriate error covariance matrices. However, the difference between the present algorithm and the one optimized for short-term variability is likely to be subtle and will show up mostly in the lower atmosphere where the algorithm is more dependent on a priori assumptions.

We have provided a detailed analysis of the information content in SBUV-derived profiles. This analysis shows that the vertical resolution of SBUV retrieved profiles varies from ~ 6 km near 3 hPa to ~ 15 km in the lower stratosphere. Though the measurements at longer SBUV wavelengths have high sensitivity to tropospheric O_3 variability, the algorithm does not have the necessary vertical resolution to separate the stratosphere from the troposphere. As a result the tropospheric variability gets distributed over a wide range of altitudes. Though this still allows the algorithm to provide very high quality total column O_3 information, some tropospheric O_3 variability aliases into the stratospheric profiles. This effect is generally small outside the tropics but can be significant in the tropical profiles.

Based on comparisons between NOAA-17 SBUV/2 with Aura MLS we find that except at higher altitudes (above 45 km) the SBUV and MLS derived O_3 anomalies

AMTD
5, 5913–5951, 2012

correlate very well after MLS anomalies are smoothed using SBUV smoothing kernels. Even without smoothing the correlations are generally quite good outside the tropics. Since MZM O_3 anomalies tend to be quite small (typically < 5 %), this comparison provides a more stringent test of the quality of SBUV measurements for climate and ozone trend studies than bias comparisons. However, bias between SBUV and smoothed-MLS is less than 5 %, part of which could be in MLS. Comparisons get worse in the tropics at altitudes where the QBO signal is dominant. This is because the SBUV vertical resolution distorts the complex vertical structure of the QBO signal. Comparisons above 45 km probably get worse due to diurnal effects caused by the 4 h local time difference between the two measurements.

Though the SBUV algorithm does not use the longer wavelengths traditionally used by total O_3 measuring instruments, such as TOMS, the quality of MZM total column O_3 derived by integrating SBUV profiles is expected to be better than TOMS. This is partly because the longest wavelength used by SBUV is always more sensitive to total O_3 variations than the 317.5 nm (331.2 nm at large SZA) wavelength used by TOMS, and partly because the total ozone derived using the SBUV algorithm at SZA > 70° is less dependent on the variations in upper stratospheric O_3 profile than the TOMS algorithm. For this reason we have used SBUV data to adjust the TOMS calibration/algorithm and plan do so for all TOMS-like total O_3 datasets produced from other instruments. Therefore these datasets should not be considered independent but complementary. While SBUV data are useful for inter-annual variability and trend studies, daily maps of total ozone produced using the TOMS algorithm are useful for process studies, and for evaluating the relative performance of ground-based total ozone measuring instruments. Based on excellent comparison with MLS of the partial O_3 columns, we highly recommend using such columns for constraining climate-chemistry models, for calculating radiative forcing, and for cross-calibrating various O_3 measuring instruments.

Although we have applied a consistent algorithm to process data from all 8 SBUV instruments, the quality of retrieved profiles from these instruments is not necessarily the same. Some instruments in the SBUV series had problems that degraded their

AMTD
5, 5913–5951, 2012

data quality and some were partially affected by two volcanic eruptions that injected aerosols in the mid stratosphere. In addition, SBUV/2 instruments on NOAA satellites have acquired data at different local times. These data are likely to be affected by local time variations in O_3 at altitudes above ~ 10 hPa. In subsequent papers we plan to provide an assessment of errors of individual instruments based on internal error analysis and comparison with other datasets.

Acknowledgements. We thank Richard Stolarski and Xiong Liu for providing valuable inputs in improving this paper, and Liang-Kang Huang for his contributions in maintaining SBUV processing software and long-term calibration.

References

Ahmad, Z. and Bhartia, P. K.: Effect of molecular anisotropy on backscattered ultraviolet radiance, Appl. Opt., 34, 8309–8314, 1995.

Ahmad, Z., Bhartia, P. K., and Krotkov, N.: Spectral properties of backscattered UV radiation in cloudy atmospheres, J. Geophys. Res.-Atmos., 109, D01201, doi:10.1029/2003jd003395, 2004.

Bass, A. M. and Paur, R. J.: The ultraviolet cross-sections of ozone, I. Measurements, in: Proc. Quad. Ozone Symp., Quad. Ozone Symp., Halkadikki, Greece, 3–7 September 1984, 606–616, 1985.

Bhartia, P. K., McPeters, R. D., Mateer, C. L., Flynn, L. E., and Wellemeyer, C.: Algorithm for the estimation of vertical ozone profiles from the backscattered ultraviolet technique, J. Geophys. Res.-Atmos., 101, 18793–18806, 1996.

Dave, J. V.: Meaning of Successive Iteration of Auxiliary Equation in Theory of Radiative Transfer, Astrophys. J., 140, 1292–1303, 1964.

Dave, J. V.: Investigation of the effect of atmospheric dust on the determination of total ozone from the earth's ultraviolet reflectivity measurements, Int. Bus. Mach. Corp., Gaithersburg, MD, 1977.

Dave, J. V.: Effect of Aerosols on Estimation of Total Ozone in an Atmospheric Column from Measurements of Its Ultraviolet Radiance, J. Atmos. Sci., 35, 809–911, 1978.

AMTD

5, 5913–5951, 2012

DeLand, M. T., Shettle, E. P., Thomas, G. E., and Olivero, J. J.: Solar backscattered ultraviolet (SBUV) observations of polar mesospheric clouds (PMCs) over two solar cycles, J. Geophys. Res.-Atmos., 108, 8445, doi:10.1029/2002JD002398, 2003.

DeLand, M. T., Taylor, S. L., Huang, L. K., and Fisher, B. L.: Calibration of the SBUV version 8.6 ozone data product, Atmos. Meas. Tech. Discuss., 5, 5151–5203, doi:10.5194/amtd-5-5151-2012, 2012.

Froidevaux, L., Jiang, Y. B., Lambert, A., Livesey, N. J., Read, W. G., Waters, J. W., Browell, E. V., Hair, J. W., Avery, M. A., Mcgee, T. J., Twigg, L. W., Sumnicht, G. K., Jucks, K. W., Margitan, J. J., Sen, B., Stachnik, R. A., Toon, G. C., Bernath, P. F., Boone, C. D., Walker, K. A., Filipiak, M. J., Harwood, R. S., Fuller, R. A., Manney, G. L., Schwartz, M. J., Daffer, W. H., Drouin, B. J., Cofield, R. E., Cuddy, D. T., Jarnot, R. F., Knosp, B. W., Perun, V. S., Snyder, W. V., Stek, P. C., Thurstans, R. P., and Wagner, P. A.: Validation of Aura Microwave Limb Sounder stratospheric ozone measurements, J. Geophys. Res.-Atmos., 113, D15s20, doi:10.1029/2007jd008771, 2008.

Haefele, A., Hocke, K., Kampfer, N., Keckhut, P., Marchand, M., Bekki, S., Morel, B., Egorova, T., and Rozanov, E.: Diurnal changes in middle atmospheric H(2)O and O(3): Observations in the Alpine region and climate models, J. Geophys. Res.-Atmos., 113, D17303, doi:10.1029/2008jd009892, 2008.

Haffner, D.: OMCLDRR Cloud pressure Climatology Summary, available at: ftp://ftp.orbit.nesdis.noaa.gov/pub/smcd/spb/ozone/Huang/test/SOLAR/OMCLDRR_clim_r4.1.pdf, 2011.

Heath, D. F., Krueger, A. J., Roeder, H. A., and Henderson, B. D.: Solar Backscatter Ultraviolet and Total Ozone Mapping Spectrometer (SBUV-TOMS) for Nimbus G, Opt. Eng., 14, 323–331, 1975.

Hilsenrath, E., Williams, D. E., Caffrey, R. T., Cebula, R. P., and Hynes, S. J.: Calibration and Radiometric Stability of the Shuttle Solar Backscatter Ultraviolet (SSBUV) Experiment, Metrologia, 30, 243–248, 1993.

Huang, F. T., Mayr, H. G., Russell, J. M., and Mlynczak, M. G.: Ozone diurnal variations in the stratosphere and lower mesosphere, based on measurements from SABER on TIMED, J. Geophys. Res.-Atmos., 115, D24308, doi:10.1029/2010jd014484, 2010.

Huang, L. K., Cebula, R. P., Taylor, S. L., Deland, M. T., McPeters, R. D., and Stolarski, R. S.: Determination of NOAA-11 SBUV/2 radiance sensitivity drift based on measurements of polar ice cap radiance, Int. J. Remote Sens., 24, 305–314, doi:10.1080/01431160304978, 2003.

AMTD
5, 5913–5951, 2012

Joiner, J., Bhartia, P. K., Cebula, R. P., Hilsenrath, E., McPeters, R. D., and Park, H.: Rotational Raman-Scattering (Ring Effect) in Satellite Backscatter Ultraviolet Measurements, Appl. Opt., 34, 4513–4525, 1995.
Klenk, K. F., Bhartia, P. K., Fleig, A. J., Kaveeshwar, V. G., McPeters, R. D., and Smith, P. M.: Total Ozone Determination from the Backscattered Ultraviolet (BUV) Experiment, J. Appl. Meteorol., 21, 1672–1684, 1982.
Kramarova, N. A., Frith, S. M., Bhartia, P. K., McPeters, R. D., and Stolarski, R.: Interpreting SBUV Smoothing Errors: An example using the Quasi-Biennial Oscillation, Atmos. Meas. Tech., in preparation, 2012.
Liu, X., Chance, K., Sioris, C. E., Spurr, R. J. D., Kurosu, T. P., Martin, R. V., and Newchurch, M. J.: Ozone profile and tropospheric ozone retrievals from the Global Ozone Monitoring Experiment: Algorithm description and validation, J. Geophys. Res.-Atmos., 110, D20307, doi:10.1029/2005JD006240, 2005.
Liu, X., Bhartia, P. K., Chance, K., Spurr, R. J. D., and Kurosu, T. P.: Ozone profile retrievals from the Ozone Monitoring Instrument, Atmos. Chem. Phys., 10, 2521–2537, doi:10.5194/acp-10-2521-2010, 2010.
Malicet, J., Daumont, D., Charbonnier, J., Parisse, C., Chakir, A., and Brion, J.: Ozone Uv Spectroscopy .2. Absorption Cross-Sections and Temperature-Dependence, J. Atmos. Chem., 21, 263–273, 1995.
McPeters, R. D.: The Behavior of Ozone near the Stratopause from 2 Years of Buv Observations, J. Geophys. Res.-Ocean. Atmos., 85, 4545–4550, 1980.
McPeters, R. D.: Climatology of Nitric Oxide in the Upper-Stratosphere, Mesosphere, and Thermosphere – 1979 through 1986, J. Geophys. Res.-Atmos., 94, 3461–3472, 1989.
McPeters, R. D.: The Atmospheric SO_2 Budget for Pinatubo Derived from NOAA-11 SBUV/2 Spectral Data, Geophys. Res. Lett., 20, 1971–1974, 1993.
McPeters, R. D. and Labow, G. J.: Climatology 2011: An MLS and sonde derived ozone climatology for satellite retrieval algorithms, J. Geophys. Res.-Atmos., 117, D10303, doi:10.1029/2011jd017006, 2012.
McPeters, R. D., Labow, G. J., and Logan, J. A.: Ozone climatological profiles for satellite retrieval algorithms, J. Geophys. Res.-Atmos., 112, D05308, doi:10.1029/2005JD006823, 2007.
Prather, M. J.: Ozone in the Upper-Stratosphere and Mesosphere, J. Geophys. Res.-Ocean. Atmos., 86, 5325–5338, 1981.

AMTD
5, 5913–5951, 2012

Rodgers, C. D.: Retrieval of Atmospheric-Temperature and Composition from Remote Measurements of Thermal-Radiation, Rev. Geophys., 14, 609–624, 1976.
Rodgers, C. D.: Characterization and Error Analysis of Profiles Retrieved from Remote Sounding Measurements, J. Geophys. Res.-Atmos., 95, 5587–5595, 1990.
Rodgers, C. D.: Inverse methods for atmospheric sounding : theory and practice, Series on atmospheric, oceanic and planetary physics, 2, World Scientific, Singapore, River Edge, N.J., XVI, p. 238, 2000.
Torres, O. and Bhartia, P. K.: Effect of Stratospheric Aerosol on Ozone Profile from Buv Measurements, Geophys. Res. Lett., 22, 235–238, 1995.
Torres, O. and Bhartia, P. K.: Impact of tropospheric aerosol absorption on ozone retrieval from backscattered ultraviolet measurements, J. Geophys. Res.-Atmos., 104, 21569–21577, 1999.
Twomey, S. A.: On the Numerical-Solution of Fredholm Integral-Equations of the 1st Kind by the Inversion of the Linear-System Produced by Quadrature, J. Assoc. Comput. Mach., 10, 97–101, 1963.
Wellemeyer, C. G., Taylor, S. L., Seftor, C. J., McPeters, R. D., and Bhartia, P. K.: A correction for total ozone mapping spectrometer profile shape errors at high latitude, J. Geophys. Res.-Atmos., 102, 9029–9038, 1997.

AMTD
5, 5913–5951, 2012

Table 1. Spectroscopic parameters for the NOAA-17 SBUV/2 sensor calculated assuming 1.1 nm triangular slit function, 1 atm = 2.148×10^{29} mols M^{-2} and 1 atm-cm = 2.687×10^{19} mols cm^{-2}. Note that the SBUV forward model accounts for variations in Rayleigh scattering coefficent with height due to change in gravity and band-averages the radiances calculated using ozone and temperature profiles for improved accuracy.

Wavelength (nm)	Rayleigh scatt coeff (atm^{-1})	Ozone sensitivity-weighted temperature, T_{eff}	Ozone abs coefficient at $T_{eff}(\alpha_{eff})$ (atm-cm^{-1})	Temp sensitivity of α_{eff} (%/K)
251.9	2.618	272.8	303	0
273.5	1.819	268.2	171	0.02
283.0	1.565	261.3	79.8	0.04
287.6	1.459	256.4	49.1	0.06
292.2	1.363	249.6	28.1	0.09
297.5	1.259	239.8	13.8	0.13
301.9	1.182	229.2	7.43	0.05
305.8	1.119	224.5	4.28	0.09
312.5	1.019	223.4	1.64	0.16
317.5	0.952	223.3	0.862	0.10
331.2	0.794	223.3	0.141	0.21
339.8	0.712	223.3	0.0245	0.58

AMTD
5, 5913–5951, 2012

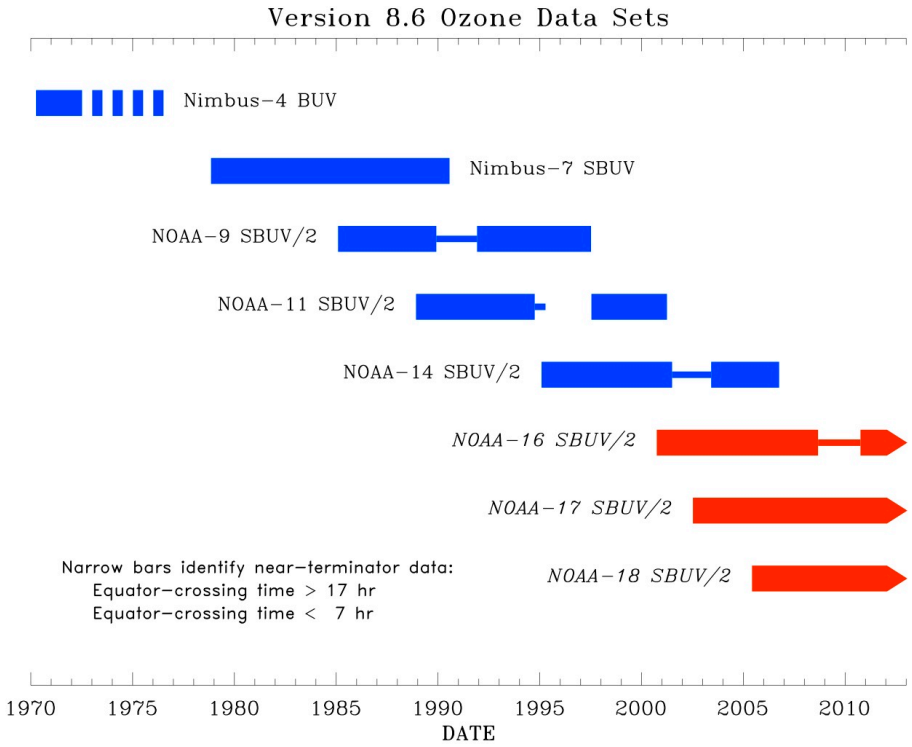

Fig. 1. Timeline of the datasets re-processed using Version 8.6 algorithm. The coverage of Nimbus-4 BUV was sparse in later years. Several NOAA instruments have missing data when the spacecraft was in a near-terminator orbit. Instruments currently operating are shown in red.

AMTD
5, 5913–5951, 2012

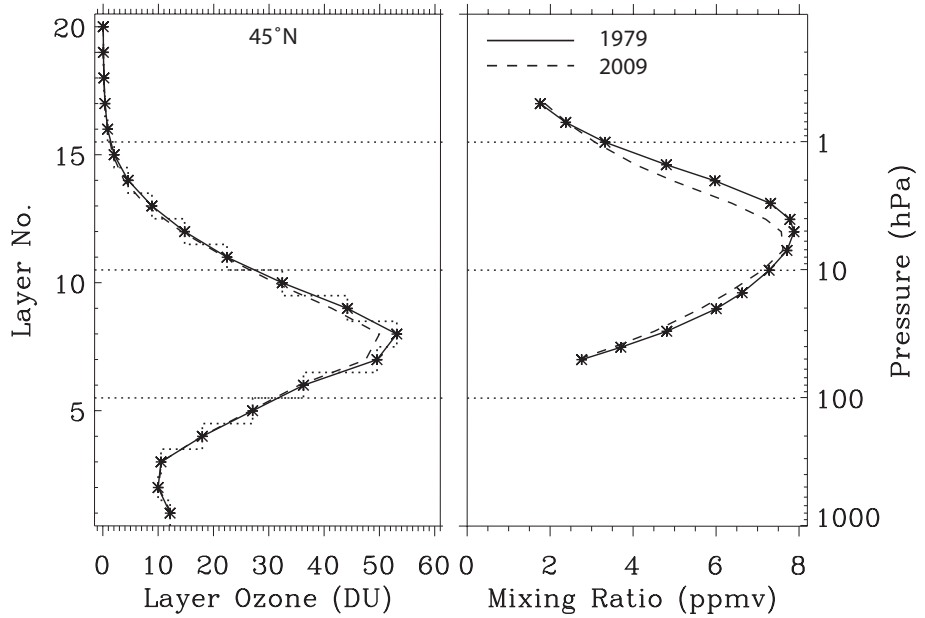

Fig. 2. Left plot shows the definition of 20 SBUV layers in pressure coordinates. The symbols show the layer mid points (in logp). The right plot shows the 15 pressure levels where ozone mixing ratios are provided in the monthly zonal mean files. The annual mean ozone profiles at 45° N latitude show significant decrease in ozone at most pressure levels over 3 decades.

AMTD
5, 5913–5951, 2012

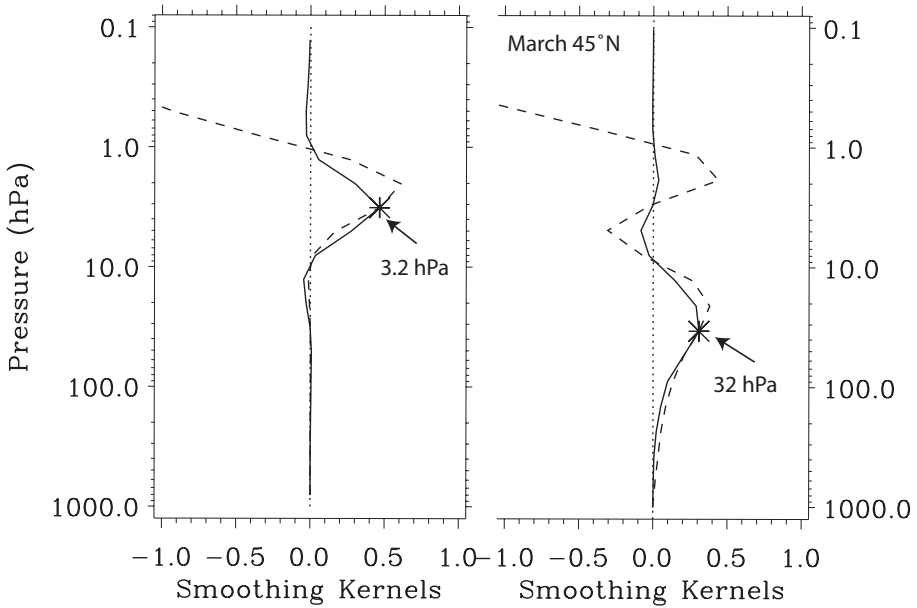

Fig. 3. SBUV smoothing kernels at 3.2 and 32 hPa for March at 45° N. The solid lines apply to fractional changes in layer ozone and the dashed line to absolute changes. We call them averaging and integrating kernels respectively. Though quite different in shape the two kernels produce mathematically the same result.

AMTD
5, 5913–5951, 2012

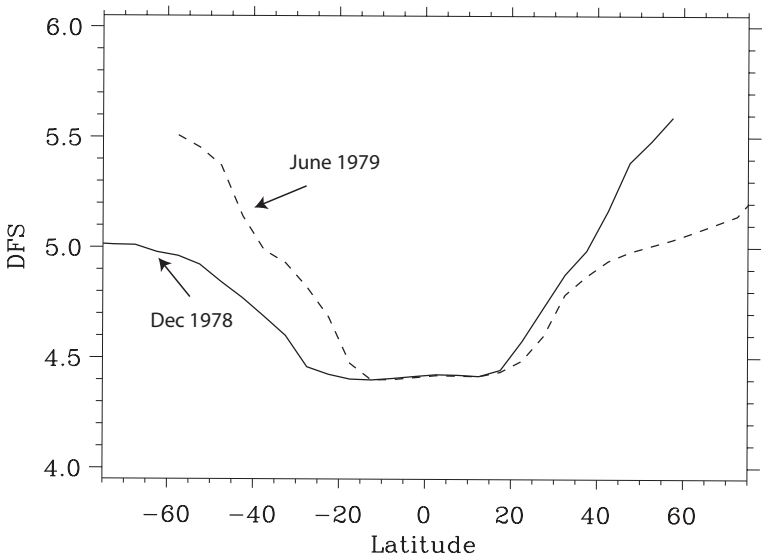

Fig. 4. Typical latitude dependence of the Degrees of Freedom of Signal (DFS). Variation in DFS are partly caused by change in solar zenith angle that changes the number of wavelengths used in the algorithm from a minimum of 6 to a maximum of 9, and partly by change in tropopause height, the higher the peak the lower the DFS. Both effects combined produce smallest DFS in the tropics.

AMTD
5, 5913–5951, 2012

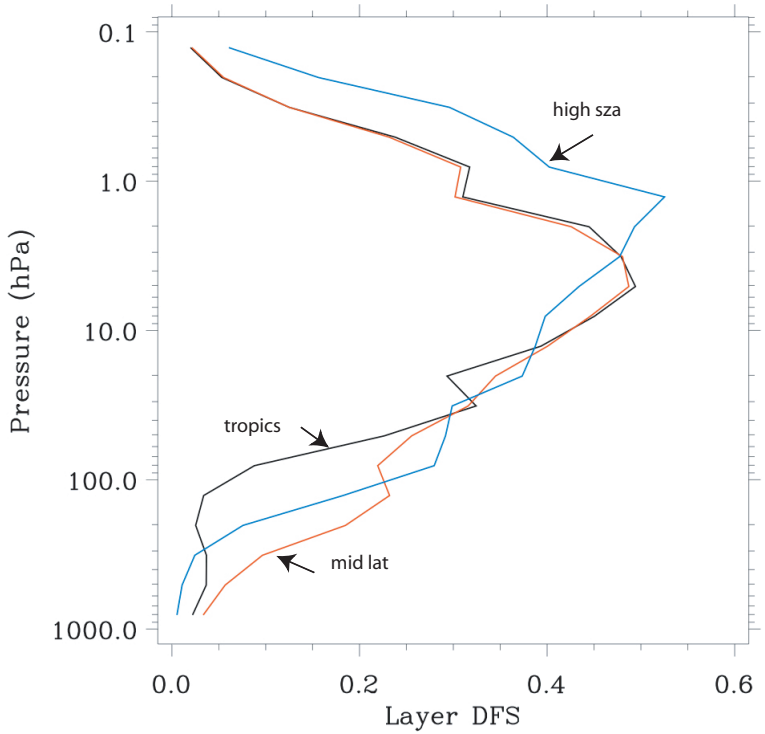

Fig. 5. Variation of layer DFS (LDFS) with height. LDFS provides the fraction of ozone change in a layer that would appear in the same layer in the retrieved profile. The vertical resolution of the retrieved profile is ~ 3.2/LDFS in km, showing that the vertical resolution varies from ~ 6 km near 3 hPa to ~ 15 km in the lower stratosphere. Lower stratospheric LDFS is largely determined by tropopause height, and the mesospheric LDFS by SZA.

AMTD
5, 5913–5951, 2012

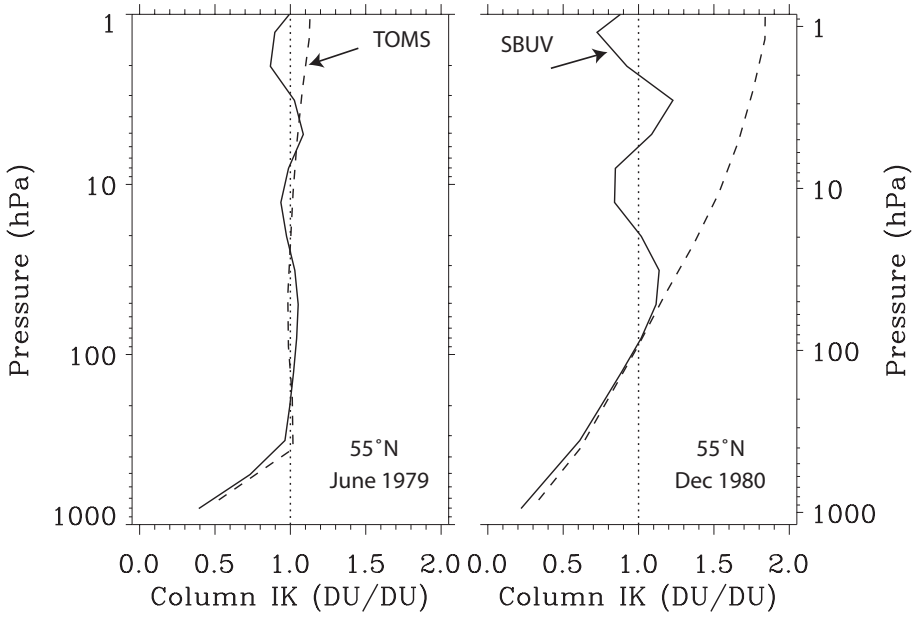

Fig. 6. Comparison of Nimbus-7 SBUV and TOMS Integrating Kernels (IK) for ozone column. Column IK provides the fraction of O_3 change in a layer that would appear in the total O_3 column of the retrieved profile. A value of 1 represents ideal sensitivity. Though TOMS uses longer wavelengths than SBUV they both have similar IKs in the summer months when solar ZA is small. But at larger SZAs (55° N in Dec) TOMS become over-sensitive to O_3 variations at higher altitudes causing increased noise in retrieved total O_3. Since theTOMS algorithm uses climatological profiles to estimate total O_3, this also causes biases when the true profile deviate from them.

AMTD
5, 5913–5951, 2012

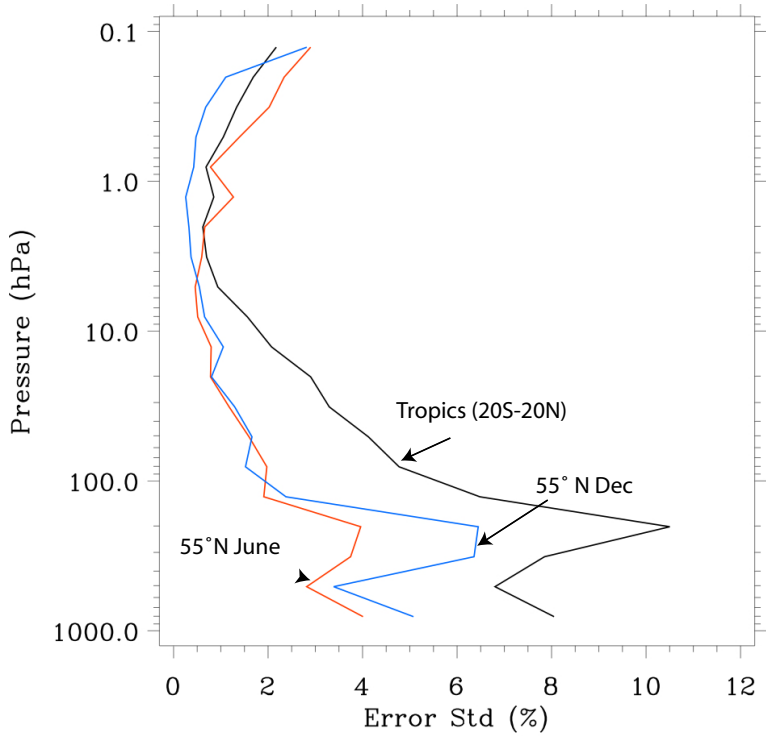

Fig. 7. Smoothing error (1σ) in estimating MZM of layer ozone. Larger errors in the tropical lower stratosphere are caused by smaller layer DFS and larger year-to-year fractional variability due to QBO. The errors shown are typically the largest source of error in estimating MZM O_3 anomalies from an SBUV instrument.

AMTD
5, 5913–5951, 2012

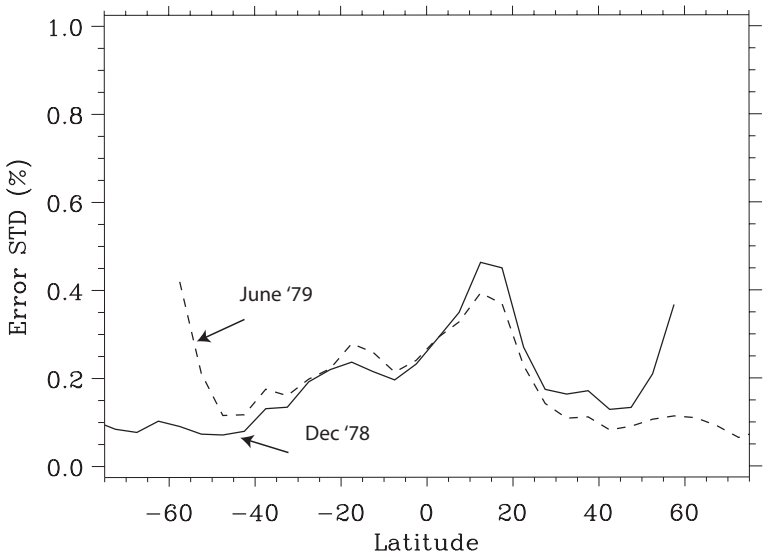

Fig. 8. Typical latitude dependence of smoothing error (1σ) in estimating MZM of total column O_3 from SBUV. These errors are caused by reduced sensitivity of the algorithm to tropospheric ozone variations seen in Fig. 6, which gets worse at larger SZAs. Larger errors in northern tropics are caused by larger inter-annual variability of tropospheric ozone. Since they are based on very limited number of ozonesonde stations, they may not be reliable.

AMTD
5, 5913–5951, 2012

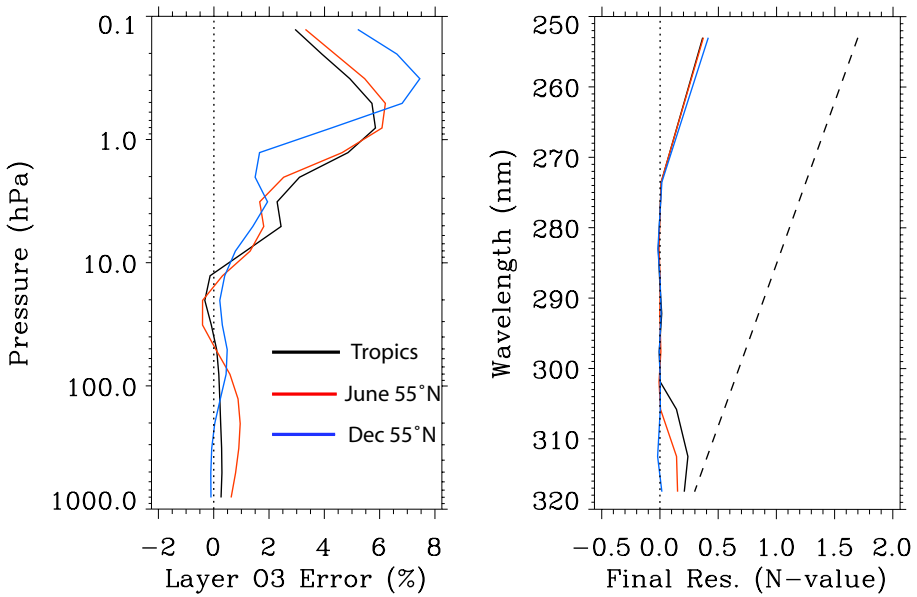

Fig. 9. Left panel shows error in layer O_3 caused by 0.05 % nm^{-1} linearly varying error in NOAA-17 SBUV radiances, assuming zero error at 331 nm (where ice radiances are used to stabilize instrument calibration) and 4 % error at 252 nm (shown as dashed line on the right panel in *N*-value unit). At higher altitudes the errors vary with SZA due to change in layer DFS shown in Fig. 5. Right panel shows the final residuals (difference from measured and calculated radiances) in *N*-value ($1N = -2.3$ %). The residuals are non-zero at wavelengths not used by the algorithm allowing one to monitor such errors.

AMTD
5, 5913–5951, 2012

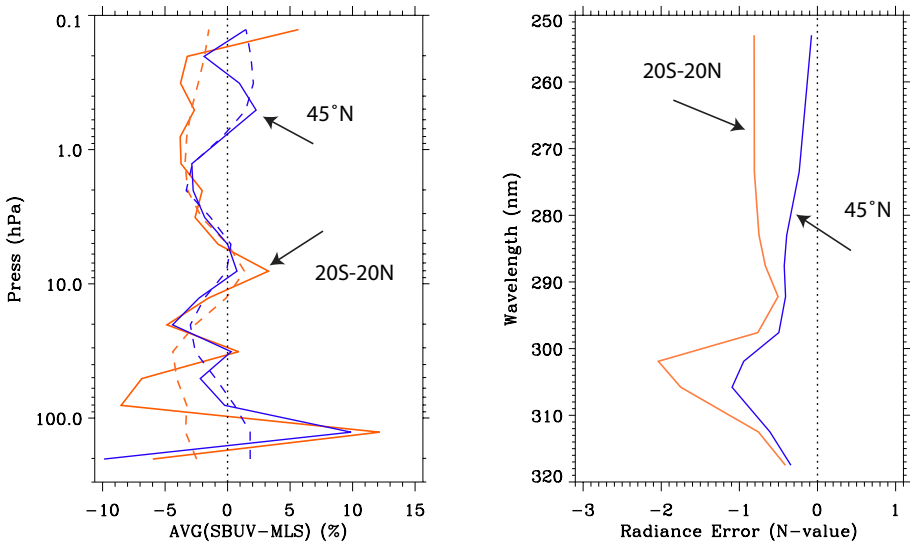

Fig. 10. Left panel shows the bias between NOAA-17/SBUV and Aura/MLS derived by averaging 6 yr of data (2005–2010). The solid lines show unsmoothed data, the dashed lines smoothed data. The smoothed differences are less than 5 % at all altitudes. Variations in unsmoothed data near 100 hPa are caused by systematic differences between MLS and ozonesonde data that were used to construct SBUV a priori. The bias at higher altitudes could be caused by diurnal effects. The right panel shows the implied error in SBUV radiances assuming MLS data have no errors. The magnitude and latitude dependence of errors at the longer wavelengths are larger than the uncertainty in SBUV measurements implying that the some of SBUV/MLS bias at lower altitudes may be MLS error.

AMTD
5, 5913–5951, 2012

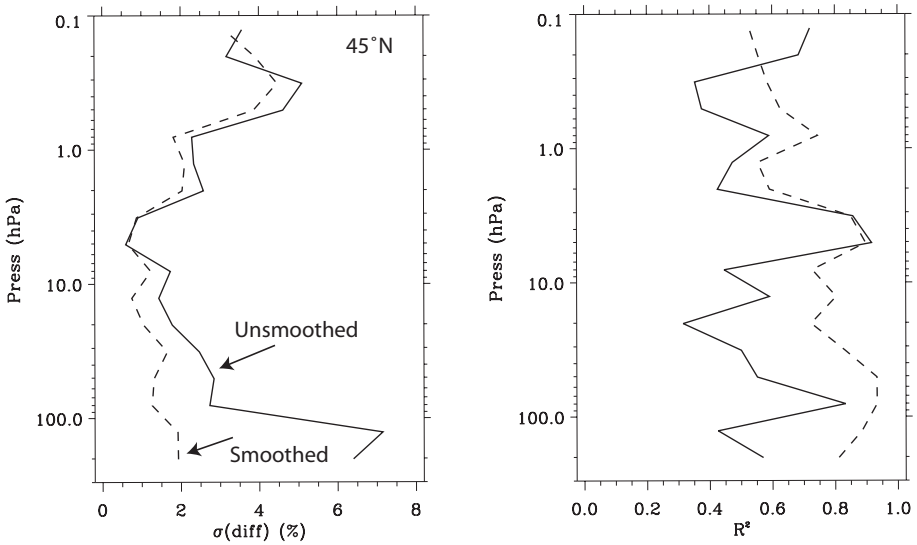

Fig. 11. Standard deviation of difference and anomaly correlation, plotted as R^2, between NOAA-17/SBUV and Aura/MLS derived using 6 yr of MZMs at 45° N (2005–2010). The solid lines show unsmoothed data, the dashed lines smoothed data. Smoothing has large effect in layers where the DFS is small, except in the mesosphere, where the diurnal effects appear to be more important.

AMTD
5, 5913–5951, 2012

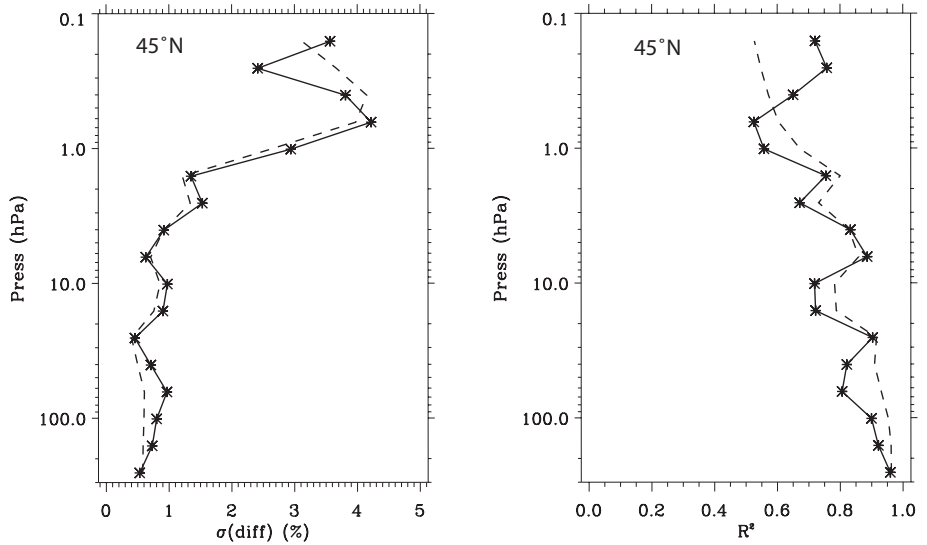

Fig. 12. Same data as used in Fig. 11, except that σ and R^2 are computed for partial column O_3 above pressure levels marked by *. Smoothing has little effect implying that SBUV can provide robust estimates of the partial column O_3 for constraining models, for providing O_3 over-burden above ozonesonde burst altitude, and for cross-calibrating satellite data. Increase in σ in the mesosphere may be due to diurnal effects.

AMTD
5, 5913–5951, 2012

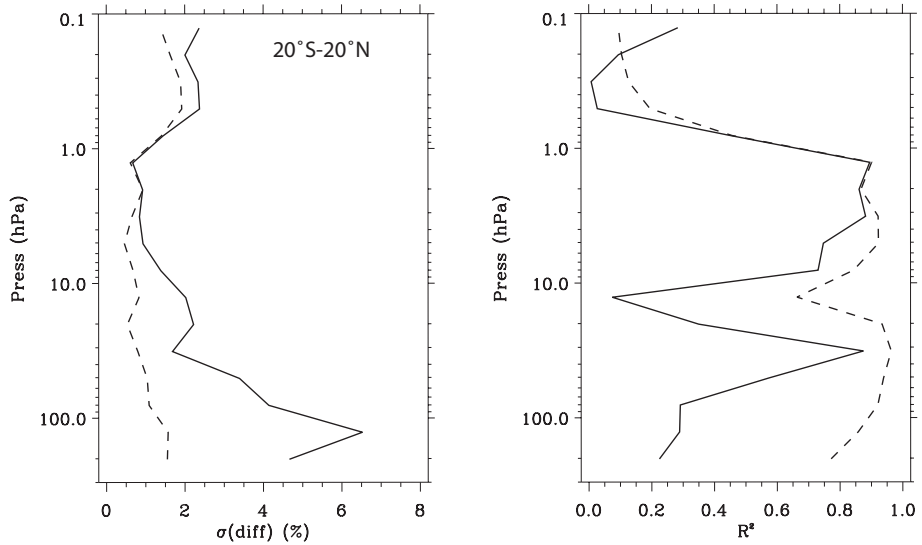

Fig. 13. Same as in Fig. 11 but for tropics (20° S–20° N). Smoothing has larger effect than at 45° N since the layer DFS is smaller in the tropics. Poor correlation in the mesosphere, even with smoothing, is probably due to diurnal effects. Poor correlation at 16 hPa is caused by distortion of the phase of the QBO by SBUV due to vertical smoothing.

AMTD
5, 5913–5951, 2012

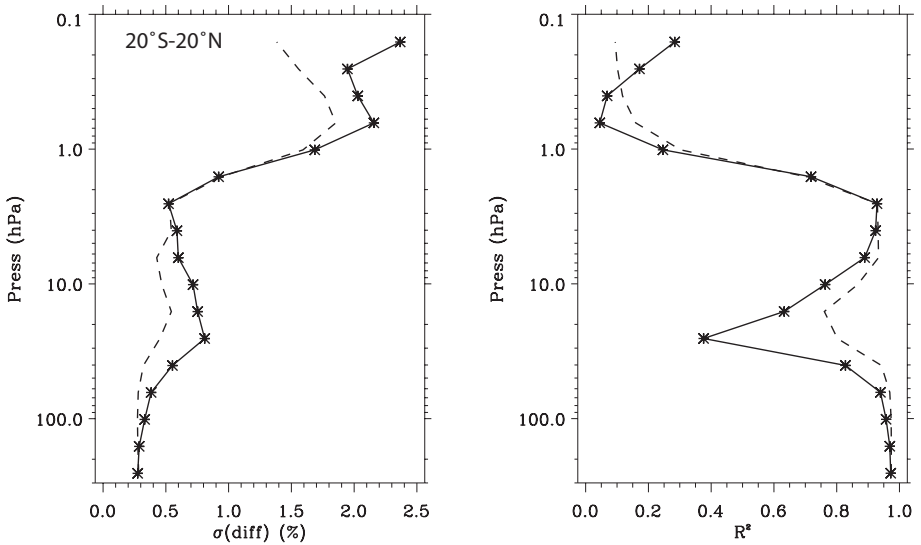

Fig. 14. Same as in Fig. 12 but for tropics (20° S–20° N). Smoothing has small effect except near 20 hPa, where errors caused by the distortion of QBO phase are still significant.

AMTD
5, 5913–5951, 2012